Indian Journal of Chemical Technology
Vol. 29, July 2022, pp. 367-379

In vitro evaluations of antimicrobial, cytotoxicity, DNA binding, cholinesterase studies of copper complexes with phenyl-selanyl ligands

P Moohambihai* & K Nagashri

Department of Chemistry, Manonmaniam Sundaranar University, Tirunelveli 627 012, Tamilnadu, India

E-mail: ambikachem12@gmail.com, shrik1810@gmail.com

Received 14 February 2022; accepted 28 April 2022

Copper (II) complexes (3a-i) with (16E)-N-(2-phenylquinolin-4(1H)-ylidine)-2-(phenylselanyl)pyridine-3-amine ligands have been synthesized. They have been characterised by various spectroscopic studies. *In-vitro* cytotoxic potential has been determined, with significant cytotoxicity against MCF-7 cell line. The copper complexes interact with the calf thymus, (CT-DNA), according to absorption spectra and viscosity measurements. In addition, the copper complexes have been tested for their antimicrobial activity against three Gram-negative bacteria; *Proteus vulgaris, Klebsiella pneumoniae, and Shigella flexneri,* three Gram-positive bacteria; *Staphylococcus aureus, Staphylococcus epidermidis, and Bacillus subtilis,* and three fungi; *Aspergillus fumigatus*, *Aspergillus clavatus* and *Candida albicans*. The ligand's acetylcholinesterase (AChE) inhibiting function has been investigated in order to determine the ligand's efficacy in the treatment of neurodegenerative disorders. When compared to standard Rivastigmine and Galantamine, the synthesised ligand 2c show selective inhibition (AChE and BuChE) with IC_{50} values of 0.19 and 3.03 µM. The egg albumin method is used to test the anti-inflammatory efficiency and α-glucosidase inhibitory activities of copper chelates are tested.

Keywords: Antimicrobial, Cytotoxicity, DNA binding, α–glucosidase, Phenylselanyl-quinoline

Schiff bases are a class of compounds that can chelate, redox active transition metal ions via the -CH=N or Ar-O- atoms[1–3]. They have a wide range of uses in pharmaceutical[4–7], catalyst[8–10], polymer synthesis, energy[11], industrial chemistry[12], and other fields. Copper, cobalt, nickel, and zinc complexes are more promising among transition metals due to their redox behaviour, low toxicity, and presence in biological molecules[13]. Chemical structural modifications of known therapeutic molecules are an important approach to the drug development process. Heterocyclic moieties, which are found in a variety of compounds, play an important role in a variety of biological processes[14]. The biological activity of these compounds is primarily determined by their molecular structures. A nitrogen-containing scaffold, quinoline core is a potent pharmacophoric moiety in existing drug molecules[15–17]. When selenium combines with quinoline, it becomes active in the research area. The selenium atom is also known to play a key role in the mode of action of certain proteins, which cannot be done by its closest relative, sulphur[18]. Synthetic organoselenium compounds have also been found to act as anti-oxidants, chemopreventers, and apoptosis inducers in a variety of organs, including the brain, liver, skin, colon, lung, and prostate[19,20]. Selenium atom is a valuable methodology for constructing a variety of five- and six-membered selenium-containing heterocyclic compounds that requires more attention. Alzheimer's disease is a progressive illness that describes a decline in cognitive capacity, memory loss, and other mental issues. In the present situation, it is the sixth most lethal disease in the world, affecting nearly 50 million people. Changes in the activities of AChE and BuChE were observed in the cerebral cortex and hippocampus and were linked to disease progression[21,22]. Many AChE inhibitors have been studied, and researchers are still working to develop some new pharmacologically profiled drug molecules[23,24]. Because of the neurotransmitter acetylcholine deficiency in the brain, AChE and BuChe levels are vary irregularly in Alzheimer's disease. With a better understanding of the relationship between AChE and BuChE levels, Alzheimer's disease can be easily tracked and managed. The majority of drugs available on the market for potential treatment of AD are cholinesterase inhibitors (Galantamine, Donepezil, Rivastigmine). Inhibitors of cholinesterase that block both AChE and BuChE, as well as highly selective BuChE inhibitors, could be useful in treating Alzheimer's disease and other dementias. Both enzymes are still important targets in therapeutic

development for Alzheimer's disease. The difficult task is always to synthesise a redox active and conjugated planar molecule with increased bioactivities against a specific target. Our study concentrated on novel cholinesterase inhibitors as potential anti-multifunctional Alzheimer's agents. The synthesis and spectroscopic elucidation of copper chelates were performed and presented in this study. Various spectroscopic techniques were used to characterise the prepared complexes. The antimicrobial, cytotoxicity, anti-inflammatory, DNA binding and α-Glucosidase inhibitory activities of phenylselanyl quinoline derivatives and their chelates were investigated.

Experimental Section

In this experiment, AnalaR grade chemicals were used. To record the NMR spectra of the ligands, tetramethylsilane (TMS) was used as an internal standard. In comparison to TMS, chemical changes (δ) are measured in parts per million. The ligands and their complexes' Fast Atom Bombardment mass spectra (FAB) were recorded on a Jeol SX 102/ DA-6000 mass spectrometer/data system with argon/xenon (6 kV, 10 mA) as the FAB gas. The molar conductance of copper complexes in dimethylsulphoxide (DMSO) solution was measured using a coronation digital conductivity meter. The IR spectra of the ligands and their copper complexes were measured in the 4000–200 cm^{-1} range using a KBr disc on a Perkin-Elmer 783 spectrophotometer. The magnetic susceptibility values were calculated using the equation eff = 2.83 (m.T)1/2. The diamagnetic adjustments were made using Pascal's constant, and the calibrant was $Hg[Co(SCN)_4]$. On a Varian E112 X-band spectrometer, the copper complexes' ESR spectra were obtained at 300 and 77 K.

Preparation of ligands 2 (a-i)

In 50 mL of DMF, 2(phenylselanyl)pyridine-3-amine was mixed with 12 mmol of sodium borohydride and stirred continuously at 0-5°C. After dilution with an equal volume of DMF, 10 mmol of phenylquinoline compounds 1(a-i) were added drop wise to the resulting solution. Reactions were completed in 60-90 minutes. The extractions were carried out in dichloromethane under vacuum. The organic layer was washed several times with brine solution before being dried over anhydrous sodium sulphate. The solvent was extracted using a rota evaporator, and the liquid was purified using a silica column and chloroform-methanol (8:2) as the eluant (Scheme 1).

2a

Yield: 71%. Anal. calcd for $C_{26}H_{17}Cl_2N_3Se$: C, 59.90; H, 3. 29; N, 8.06; Found: C, 59.86; H, 3.25; N, 8.02. FAB mass spectrometry (FAB-MS) m/z 522 [M+1]. ^1H NMR (400 MHz, $CDCl_3$, δ, ppm): 6.32 (s,

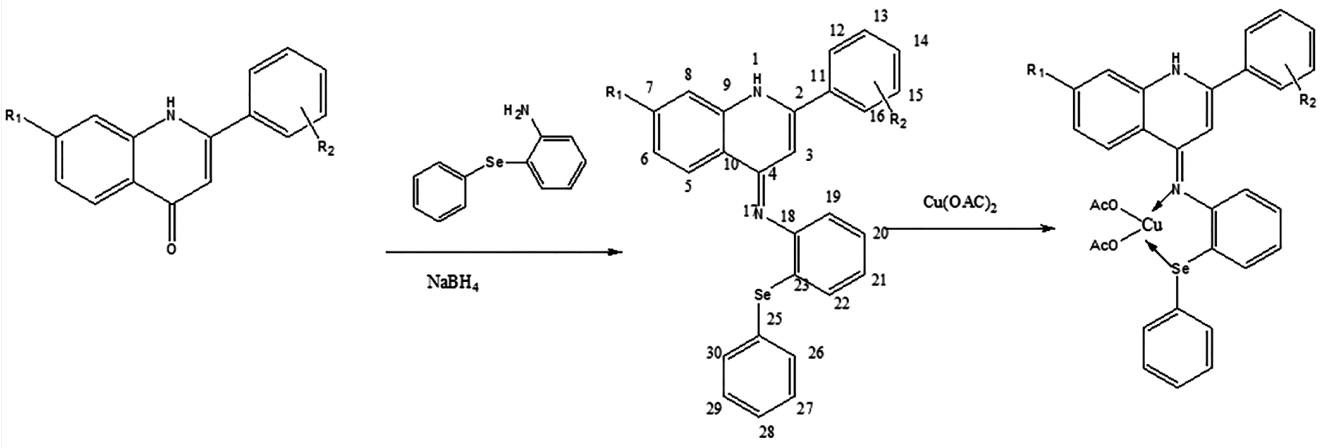

1a-i

1a, R_1 = H, R_2 = 2, 4-dichloro
1b, R_1 = H, R_2 = 2, 6-dichloro
1c, R_1 = Cl, R_2 = 2, 4-dichloro
1d, R_1 = Cl, R_2 = 2, 6-dichloro
1e, R_1 = OH, R_2 = 2, 4-dichloro
1f, R_1 = OH, R_2 = 2, 6-dichloro
1g, R_1 = Cl, R_2 = H
1h, R_1 =OH, R_2 = H
1i, R_1 = H, R_2 = H

2a-i

2a, R_1 = H, R_2 = 2, 4-dichloro
2b, R_1 = H, R_2 = 2, 6-dichloro
2c, R_1 = Cl, R_2 = 2, 4-dichloro
2d, R_1 = Cl, R_2 = 2, 6-dichloro
2e, R_1 = OH, R_2 = 2, 4-dichloro
2f, R_1 = OH, R_2 = 2, 6-dichloro
2g, R_1 = Cl, R_2 = H
2h, R_1 =OH, R_2 = H
2i, R_1 = H, R_2 = H

3a-i

3a, R_1 = H, R_2 = 2, 4-dichloro
3b, R_1 = H, R_2 = 2, 6-dichloro
3c, R_1 = Cl, R_2 = 2, 4-dichloro
3d, R_1 = Cl, R_2 = 2, 6-dichloro
3e, R_1 = OH, R_2 = 2, 4-dichloro
3f, R_1 = OH, R_2 = 2, 6-dichloro
3g, R_1 = Cl, R_2 = H
3h, R_1 =OH, R_2 = H
3i, R_1 = H, R_2 = H

Scheme —1

1H), 6.34-6.58 (m, 4H), 7.18 (s, 1H), 7.16 (d, 1H), 7.14 (d, 1H), 7.20-7.40 (m, 3H), 7.42-7.48(d, 2H), 7.50-7.58 (m, 3H), 9.24 (s, -NH). ^{13}C NMR (400 MHz, DMSO-d_6): 138.8 (C-2), 102.1 (C-3), 164.6 (C-4), 130.1 (C-5), 118.8 (C-6), 131.8 (C-7), 116.3 (C-8), 148.1 (C-9), 117.7 (C-10), 133.4 (C-11), 129.2 (C-12), 126.9 (C-13), 134.9 (C- 14), 130.3 (C-15). 132.6 (C-16), 153.1 (C-18), 122.3 (C-19), 130.2 (C-20), 127.2 (C-21), 142.8 (C-23), 130.0 (C-25), 131.5 (C-26, C-30), 128.7 (C-27, C-28, C-29).

2b

Yield: 75 %. Anal. calcd for $C_{26}H_{17}Cl_2N_3Se$: C, 59.90; H, 3. 29; N, 8.06; Found: C, 59.85; H, 3.24; N, 8.01. FAB mass spectrometry (FAB-MS) m/z 522 [M+1]. ^{1}H NMR (400 MHz, $CDCl_3$, δ, ppm): 6.35 (s, 1H), 6.34 -6.58 (m,4H), 7.18 (s, 1H), 7.16 (d, 1H), 7.14 (d, 1H), 7.20-7.40 (m, 3H), 7.42-7.48(d, 2H), 7.50-7.58 (m, 3H), 9.24 (s, -NH). ^{13}C NMR (400 MHz, DMSO-d_6): 138.8 (C-2), 102.1 (C-3), 164.6 (C-4), 131.1 (C-5), 105.8 (C-6), 131.8 (C-7), 101.1 (C-8), 148.3 (C-9), 110.2 (C-10), 133.4 (C-11), 122.2 (C-12, C-16), 126.9 (C-13, C-15), 130.9 (C-14), 153.1 (C-18), 122.3 (C-19), 130.2 (C-20), 127.2 (C-21), 142.8 (C-23), 130.0 (C-25), 131.5 (C-26, C-30), 128.7 (C-27, C-28, C-29).

2c

Yield: 70 %. Anal. calcd for $C_{26}H_{16}Cl_3N_3Se$: C, 56.19; H, 2.90; N, 7.56; Found: C, 56.16; H, 2.85; N, 7.52. FAB mass spectrometry (FAB-MS) m/z 556 [M+1]. ^{1}H NMR (400 MHz, $CDCl_3$, δ, ppm): 6.32 (s, 1H), 6.34 (d,1H), 6.42 (d,1H), 6.54 (s,1H) 7.18 (s, 1H), 7.16 (d, 1H), 7.14 (d, 1H), 7.20-7.40 (m, 3H), 7.42-7.48(d, 2H), 7.50-7.58 (m, 3H), 9.28 (s, -NH). ^{13}C NMR (400 MHz, DMSO-d_6): 138.8 (C-2), 102.1 (C-3), 164.6 (C-4), 131.2 (C-5), 118.8 (C-6), 131.8 (C-7), 116.3 (C-8), 148.1 (C-9), 117.7 (C-10), 133.4 (C-11), 129.2 (C-12), 126.9 (C-13), 134.9 (C- 14), 130.3 (C-15). 132.6 (C-16), 153.1 (C-18), 122.3 (C-19), 130.2 (C-20), 127.2 (C-21), 142.8 (C-23), 130.0 (C-25), 131.5 (C-26, C-30), 128.7 (C-27, C-28, C-29).

2d

Yield: 72 %. Anal. calcd for $C_{26}H_{16}Cl_3N_3Se$: C, 56.19; H, 2.90; N, 7.56; Found: C, 56.16; H, 2.85; N, 7.52. FAB mass spectrometry (FAB-MS) m/z 556 [M+1]. ^{1}H NMR (400 MHz, $CDCl_3$, δ, ppm): 6.32 (s, 1H), 6.34 (d,1H), 6.42 (d,1H), 6.54 (s,1H) 7.14 (d, 2H), 7.18 (t, 1H), 7.20-7.40 (m, 3H), 7.42-7.48(d, 2H), 7.50-7.58 (m, 3H), 9.28 (s, -NH). ^{13}C NMR (400 MHz, DMSO-d_6): 138.8 (C-2), 102.1 (C-3), 164.6 (C-4), 131.1 (C-5), 105.8 (C-6), 131.8 (C-7), 101.1 (C-8), 148.3 (C-9), 110.2 (C-10), 133.4 (C-11), 122.2 (C-12, C-16), 126.9 (C-13, C-15), 130.9 (C- 14), 130.3 (C-15). 153.1 (C-18), 122.3 (C-19), 130.2 (C-20), 127.2 (C-21), 142.8 (C-23), 130.0 (C-25), 131.5 (C-26, C-30), 128.7 (C-27, C-28, C-29).

2e

Yield: 73 %. Anal. calcd for $C_{26}H_{17}Cl_2N_3OSe$: C, 58.12; H, 3.19; N, 7.82; Found: C, 58.09; H, 3.15; N, 7.81. FAB mass spectrometry (FAB-MS) m/z 538 [M+1]. ^{1}H NMR (400 MHz, $CDCl_3$, δ, ppm): 6.10 (s, 1H), 6.22 (d, 1H), 6.32 (d, 1H), 6.36 (s, 1H), 7.10 (s, 1H), 7.12 (d, 1H), 7.14 (d, 1H), 7.18-7.32 (m, 3H), 7.40-7.46 (d, 2H), 7.52-7.62 (m, 3H), 9.22 (s, -NH), 9.94 (s, -OH). ^{13}C NMR (400 MHz, DMSO-d_6): 138.8 (C-2), 102.1 (C-3), 164.6 (C-4), 131.1 (C-5), 105.8 (C-6), 131.8 (C-7), 101.1 (C-8), 148.3 (C-9), 110.2 (C-10), 133.4 (C-11), 129.2 (C-12), 126.9 (C-13), 134.9 (C- 14), 130.3 (C-15). 132.6 (C-16), 153.1 (C-18), 122.3 (C-19), 130.2 (C-20), 127.2 (C-21), 142.8 (C-23), 130.0 (C-25), 131.5 (C-26, C-30), 128.7 (C-27, C-28, C-29).

2f

Yield Yield: 70 %. Anal. calcd for $C_{26}H_{17}Cl_2N_3OSe$: C, 58.12; H, 3.19; N, 7.82; Found: C, 58.08; H, 3.14; N, 7.81. FAB mass spectrometry (FAB-MS) m/z 538 [M+1]. ^{1}H NMR (400 MHz, $CDCl_3$, δ, ppm): 6.10 (s, 1H), 6.22 (d, 1H), 6.32 (d, 1H), 6.36 (s, 1H), 7.12 (d, 2H), 7.16 (t, 1H), 7.18-7.32 (m, 3H), 7.40-7.46 (d, 2H), 7.52-7.62 (m, 3H), 9.22 (s, -NH), 9.88 (s, -OH). ^{13}C NMR (400 MHz, DMSO-d_6): 138.8 (C-2), 102.1 (C-3), 164.6 (C-4), 131.1 (C-5), 105.8 (C-6), 131.8 (C-7), 101.1 (C-8), 148.3 (C-9), 110.2 (C-10), 133.4 (C-11), 122.2 (C-12, C-16), 126.9 (C-13, C-15), 130.9 (C- 14), 130.3 (C-15). 153.1 (C-18), 122.3 (C-19), 130.2 (C-20), 127.2 (C-21), 142.8 (C-23), 130.0 (C-25), 131.5 (C-26, C-30), 128.7 (C-27, C-28, C-29).

2g

Yield: 71 %. Anal. calcd for $C_{26}H_{18}ClN_3Se$: C, 64.14; H,3.73; N, 8.63; Found: C, 66.11; H, 3.70; N, 8.59. FAB mass spectrometry (FAB-MS) *m/z* 488 [M+1]. ^{1}H NMR (400 MHz, $CDCl_3$, *δ*, ppm): 6.12 (s, 1H), 6.34 (d, 1H), 6.42 (d, 1H), 6.54 (s, 1H), 6.94-7.24 (m, 5H), 7.28-7.40, 7.42-7.46 (d, 2H), 7.52-7.62 (m, 3H), 9.22 (s, -NH). ^{13}C NMR (400 MHz, DMSO-d_6): 138.1 (C-2), 102.1 (C-3), 164.6 (C-4), 131.4 (C-

5), 119.1 (C-6), 137.4 (C-7), 110.8 (C-8), 149.5 (C-9), 115.9(C-10), 138.2 (C-11), 126.3 (C-12, C-16), 128.6 (C-13, C-15), 128.0 (C-14), 153.1 (C-18), 122.3 (C-19), 130.2 (C-20), 127.2 (C-21), 142.8 (C-23), 130.0 (C-25), 131.5 (C-26, C-30), 128.7 (C-27, C-28, C-29).

2h

Yield: 74 %. Anal. calcd for $C_{26}H_{19}N_3OSe$: C, 66.67; H, 4.09; N, 8.97; Found: C, 66.63; H, 4.05; N, 8.95. FAB mass spectrometry (FAB-MS) *m/z* 469 [M+1]. ^{1}H NMR (400 MHz, $CDCl_3$, δ, ppm): 6.10 (s, 1H), 6.25 (d, 1H), 6.40 (d, 1H), 6.52 (s, 1H), 6.94-7.24 (m, 5H) 7.28-7.40 (m, 3H), 7.42-7.46 (d, 2H), 7.50-7.60 (m, 3H), 9.22 (s, -NH), 10.12 (s, 1H). ^{13}C NMR (400 MHz, DMSO-d_6): 138.1 (C-2), 102.1 (C-3), 164.6 (C-4), 131.4 (C-5), 106.1 (C-6), 161.6 (C-7), 101.2 (C-8), 149.5 (C-9), 115.9(C-10), 134.2 (C-11), 126.3 (C-12, C-16), 128.6 (C-13, C-15),128.1 (C-14), 153.1 (C-18), 122.3 (C-19), 130.2 (C-20), 127.2 (C-21), 142.8 (C-23), 130.0 (C-25), 131.5 (C-30-26, C), 128.7 (C-27, C-28, C-29).

2i

Yield Yield: 74 %. Anal. calcd for $C_{26}H_{19}N_3Se$: C, 69.03; H, 4.23; N, 8.97; Found: C, 69.02; H, 4.21; N, 8.93. FAB mass spectrometry (FAB-MS) *m/z* 453 [M+1]. ^{1}H NMR (400 MHz, $CDCl_3$, δ, ppm): 6.32 (s, 1H), 6. 52-7.22 (m, 4H), 6.94-7.22 (m, 5H) 7.24-7.40(m, 3H), 7.42-7.46 (d, 2H), 7.52-7.62 (m, 3H), 9.22 (s, -NH) ^{13}C NMR (400 MHz, DMSO-d_6): 138.9 (C-2), 102.1 (C-3), 164.6 (C-4), 130.0 (C-5), 118.8 (C-6), 131.8 (C-7), 116.3 (C-8), 148.1 (C-9), 117.7 (C-10), 134.2 (C-11), 126.3 (C-12, C-16), 128.6 (C-13, C-15), 128.1 (C-14), 153.1 (C-18), 122.3 (C-19), 130.2 (C-20), 127.2 (C-21), 142.8 (C-23), 130.0 (C-25), 131.5 (C-26, C-30), 128.7 (C-27, C-28, C-29).

Prearation of metal chelates [3a-i ($CuL^1(OAc)_2$ - $CuL^9(OAc)_2$)]

Equimolar hot ethanolic solutions of phenylselanylquinoline derivative and copper acetate (0.05 M) were placed in a RB flask at room temperature, the reacting mixture was stirred and allowed to precipitate. The solid product was then separated with methanol and hexane and washed repeatedly. The remaining metal complexes were prepared with the same procedure. The metal chelates were dried in a vacuum desiccator over fused calcium chloride.

3a ($CuL^1(OAc)_2$): Yield: 70%. Anal. calcd for $C_{30}H_{23}Cl_2CuN_3O_4Se$: C, 51.26, H, 3.30; N, 5.98; Found: C 51.23; H 3.26; N 5.96. FTIR (KBr): 1638 ν (C=N), 500-540 ν (Cu–N). FAB mass: 704 m/z [M+1]. μ_{eff} (BM) = 1.86; Δ_m (mho cm^2 mol^{-1}) = 18.

3b ($CuL^2(OAc)_2$): Yield: 70%. Anal. calcd for $C_{30}H_{23}Cl_2CuN_3O_4Se$: C, 51.26, H, 3.30; N, 5.98; Found: C 51.24; H 3.25; N 5.95. FTIR (KBr): 1638 ν(C=N), 500-540 ν(Cu–N). FAB mass: 704 m/z [M+1] μ_{eff} (BM) = 1.86; Δ_m (mho cm^2 mol^{-1}) = 16.

3c ($CuL^3(OAc)_2$): Yield: 75%. Anal. calcd for $C_{30}H_{22}Cl_3CuN_3O_4Se$: C, 48.87, H, 3.01; N, 5.70; Found: C 48.84; H 3.26; N 5.96. FTIR (KBr): 1638 ν (C=N), 500-540 ν (Cu–N). FAB mass: 738 m/z [M+1] μ_{eff} (BM) = 1.86; Δ_m (mho cm^2 mol^{-1}) = 14.

3d ($CuL^4(OAc)_2$): Yield: 72%. Anal. calcd for $C_{30}H_{22}Cl_3CuN_3O_4Se$: C, 48.87, H, 3.01; N, 5.70; Found: C 48.83; H 3.27; N 5.96. FTIR (KBr): 1638 ν (C=N), 500-540 ν(Cu–N). FAB mass: 738 m/z [M+1] μ_{eff} (BM) = 1.86; Δ_m (mho cm^2 mol^{-1}) = 18.

3e ($CuL^5(OAc)_2$): Yield: 69%. Anal. calcd for $C_{30}H_{23}Cl_2CuN_3O_5Se$: C, 50.18, H, 3.22; N, 5.84; Found: C 50.14; H 3.18; N 5.81. FTIR (KBr): 3310 ν (O–H), 1638 ν (C=N), 500-540 ν (Cu–N). FAB mass: 720 m/z [M+1] μ_{eff} (BM) = 1.86; Δ_m (mho cm^2 mol^{-1}) = 16.

3f ($CuL^6(OAc)_2$): Yield: 71%. Anal. calcd for $C_{30}H_{23}Cl_2CuN_3O_5Se$: C, 50.18, H, 3.22; N, 5.84; Found: C 50.15; H 3.19; N 5.82. FTIR (KBr): 3310 ν (O–H), 1638 ν (C=N), 500-540 ν (Cu–N). FAB mass: 720 m/z [M+1] μ_{eff} (BM) = 1.86; Δ_m (mho cm^2 mol^{-1}) = 14.

3g ($CuL^7(OAc)_2$): Yield: 68%. Anal. calcd for $C_{30}H_{24}ClCuN_3O_4Se$: C 53.90, H 3.62, N 6.29, Found: C 53.86, H 3.60, N 6.25. FTIR (KBr):1632 ν(C=N), 550 ν(Cu–N). FAB mass: 669 m/z [M+1]. μ_{eff} (BM) = 1.86; Δ_m (mho cm^2 mol^{-1}) = 18.

3h ($CuL^8(OAc)_2$): Yield: 67%. Anal. calcd for $C_{30}H_{25}CuN_3O_5Se$: C 55.43, H 3.88, N 6.46; Found: C 55.41, H 3.85, N 6.43. FTIR (KBr): 3310 ν(O–H), 1632 ν(C=N), 550 ν(Cu–N). FAB mass: 651 m/z [M+1]. μ_{eff} (BM) = 1.86; Δ_m (mho cm^2 mol^{-1}) = 20.

3i ($CuL^9(OAc)_2$): Yield: 69%. Anal. calcd for $C_{30}H_{25}CuN_3O_4Se$: C 56.83, H 3.57, N 6.63; Found: C 56.79, H 3.54, N 6.61. FTIR (KBr): 1632 ν(C=N),

550 ν(Cu–N). FAB mass: 635 m/z [M+1]. μ_{eff} (BM) = 1.96; Δ_m (mho cm^2 mol^{-1}) = 20.

Results and Discussion

All copper complexes are stable at room temperature, insoluble in water but soluble in DMSO and Methylcyanide. On the isolated solid complexes of Cu(II) ion with the ligands, elemental analyses (C, H, and N), IR, magnetic moments, molar conductance, ^{1}H NMR, and ESR were performed to understand the molecular structures of copper complexes. Analytical data from the ligands and their complexes were used to develop the empirical formula for the ligands and their complexes. TLC was used to compare the synthesised ligands to the starting materials. All complexes generated excellent elemental analysis results within the limits of experimental error (as shown in the Experimental section). All compounds disintegrated above 250°C, indicating their thermal stability[25-27].

IR spectra

The IR spectra of the ligands show a ν (C=N) peak in the 1654–1632 cm^{-1} range. All complexes have ν (C= N) bands at 1639–1580 cm^{-1} in their IR spectra[28], which are relocated to lower energy areas in the complexes compared to the free ligands. The change in the energy side of this band is most likely owing to an increase in the C=N bond order caused by the coordination of nitrogen with the copper atom. Complex spectra, exhibit two distinct bands attributable to ν_{asy} (COO^-) and ν_{sy} (COO^-) at 1630–1600 and 1404–1340 cm^{-1}, respectively. Indicating that the complexes include the carboxylate oxygen atom. The degree of separation between the ν_{asy} (COO^-) and ν_{sy} (COO^-) has also been utilised to determine the carboxylate group coordination mode. In copper complexes, the separation value between ν_{asy} (COO^-) and ν_{sy} (COO^-) was larger than 200 cm^{-1}, indicating that the carboxylate group in copper complexes of the ligands is coordinated monodentately[29]. Furthermore, the formation of complexes was also ascertained by the presence of medium intensity bands at 576–578 cm^{-1} and 468–470 cm^{-1}, which were assigned to ν (M-O) and ν (M-N), respectively[30]. Table 1 shows the characteristic peaks of ligands and complexes.

Mass spectra

The structure of a substance can also be determined by mass spectra. The mass spectra of the ligand (2c) and its copper complex [$CuL^3(OAc)_2$] were recorded and their stoichiometric compositions were compared, as shown in Figs 1(a) and 1(b). The ion's stability and abundance are reflected in the intensity of these peaks[31]. The ligand (2c) has a molecular ion peak at 556 m/z, whereas its copper complex has a molecular ion peak at 738 m/z, indicating that the copper complexes have 1:1 stoichiometry. Elemental analysis values resemble those estimated from molecular

Table 1 — IR characteristic peaks of synthesized ligands and complexes

Ligand / complex	ν C=N (cm^{-1})	ν M-N (cm^{-1})	ν (coo^-)$_{ass}$ (cm^{-1})	ν (coo^-)$_{sy}$ (cm^{-1})
2a	1635	-	-	-
2b	1630		-	-
2c	1622	-	-	-
2d	1629	-	-	-
2e	1610	-	-	-
2f	1635	-	-	-
2g	1625	-	-	-
2h	1612	-	-	-
2i	1622	-	-	-
3a	1625	520 – 550	1615	1380
3b	1620	530 – 550	1610	1370
3c	1610	520 – 550	1600	1390
3d	1620	530 – 550	1610	1370
3e	1620	520 – 550	1610	1380
3f	1625	520 – 550	1615	1350
3g	1615	530 – 550	1600	1380
3h	1610	520 – 550	1600	1370
3i	1590	530 – 550	1610	1400

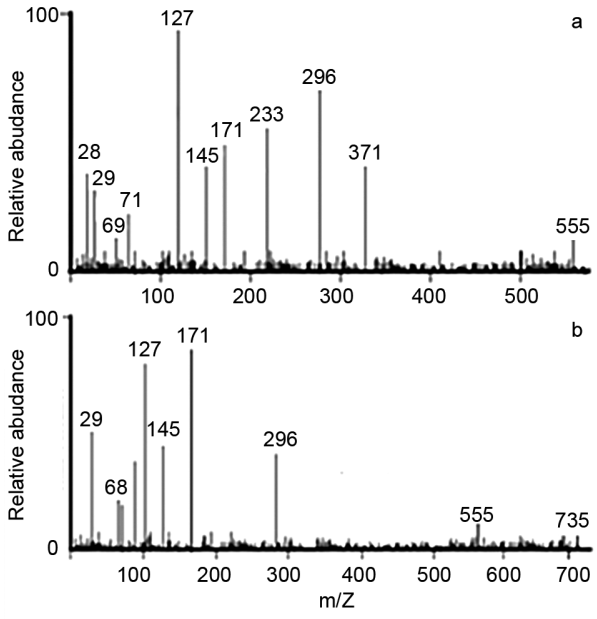

Fig. 1 — (a) Mass spectrum of ligand 2c and (b) Mass spectrum of copper complex 3c

formulae assigned to these complexes, as evidenced by FAB-mass examinations of individual complexes. Similar mass spectral features were given to other ligands and their copper complexes.

^{1}H-NMR spectra

The experimental part contains the ^{1}H and ^{13}C-NMR spectra of ligands recorded in $CDCl_3$. Ligand 2c exhibits 6.12 (s, 1H), 6.34 (d, 1H), 6.42 (d, 1H), 6.54 (s, 1H), 7.12 (s, 1H), 7.18 (d, 1H), 7.20 (d, 1H), 7.22-7.36 (m, 4H), 7.43-7.50 (d, 2H), 7.52-7.62 (m, 3H), 9.22 (s, -NH). All of the protons were discovered to be in the expected location[32]. The findings of this research add to the evidence for the bonding mode indicated in their IR spectra. The number of protons calculated from the integration curves and those calculated from the predicted CHN analysis values accord.

Electronic spectra

In DMSO as a solvent, the electronic spectra of the ligands and their complexes were recorded. The absorption spectra of the ligand show bands at 224 and 312 nm due to n– π * and π – π * transitions within the Schiff base molecule. The electronic spectra of the analogous complex in DMSO reveal a band at 556 nm that may be given to the $^2B_{1g} \rightarrow {}^2A_{1g}$ transition[33,34]. This band is suggestive of the square planar environment around the copper (II) ion and can be assigned to the $^2B_{1g} \rightarrow {}^2A_{1g}$ transition. Other compounds were given similar spectral characteristics. The benzenoid's π – π * transition / or n– π * (COO), the > C=N- chromophore's π – π * transition, and the > C=N- chromophore's n– π * transition, along with the secondary band of the benzene, display bands in the 200–225, 272–332 and 362–390 nm ranges in the electronic spectra of all the complexes. Furthermore, there were a few sharp lines in the complexes' spectra in the 233–257 nm range that could indicate charge transfer bands. At ambient temperature, magnetic susceptibility experiments revealed that the copper complexes were paramagnetic. The magnetic moments of these complexes are extremely comparable to those of copper (II) complexes with no metal–metal interaction. At room temperature, the magnetic moment of the complex 3c is 1.86 BM, which is characteristic of mononuclear complexes of magnetically diluted d^9 systems with S = 1/2 spin state and square planar structure, with no metal–metal interaction along the axial position. Other copper complexes had comparable magnetic properties (Fig. 2).

ESR spectra

Copper chelate ESR spectra (Fig. 3) collected at 77 K in DMSO solution. It was found to have a g|| value of 2.262, indicating that the metal-ligand link was a covalent [35]. It was calculated that the planar distortion of copper (II) chelate due to regular geometrical arrangements (f = g||/A||) is 146.2. The results demonstrated that the biomolecular mechanism for biological reactions was facilitated by the distortion caused by regular square planar geometry around the copper centre[36].

Molar conductance

For the 0.001 M solutions found in the experimental section, the molar conductance data for the copper complexes measured in DMSO solution. The complexes had values ranging from 10 to 29 mho cm^2 mol^{-1}, which is within the expected

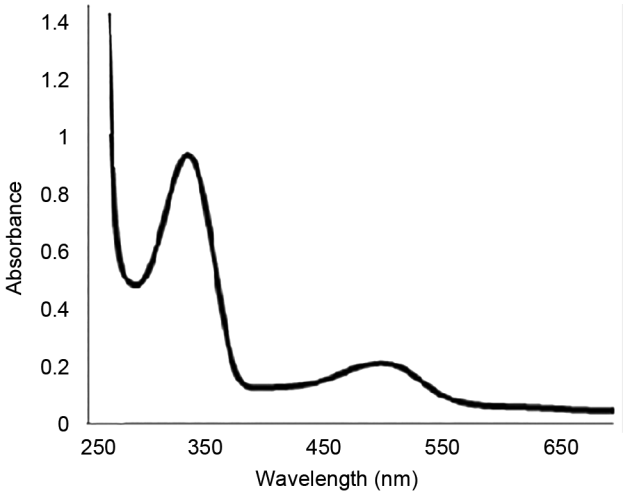

Fig. 2 — UV spectrum of copper complex 3c

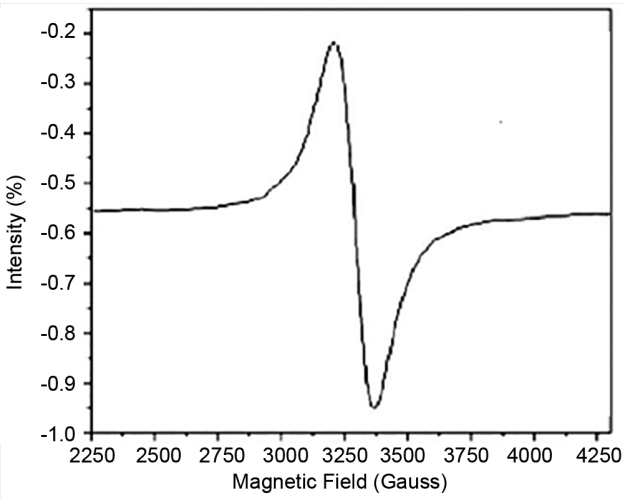

Fig. 3 — ESR spectrum of copper complex 3c

range of 1 to 35 mho cm^2 mol^{-1} for non-electrolytes[37]. Because of the involvement of the acetate groups in coordination, the complexes are non-electrolytic. A chemical analysis of the CH_3COO^- ion that was not precipitated by the addition of $FeCl_3$ confirmed this.

TGA and DTA studies

The TGA and DTA curves of the Cu (II) complex (Fig. 4) revealed that the complex is stable up to 250°C, with no weight loss before this temperature. At 250°C, the first stage of deterioration began with the loss of three chlorine atoms, resulting in an 11.95 % functional weight loss. At 291°C, further degradation of the resultant complex resulted in the loss of the phenyl moiety, resulting in a functional weight loss of 11.40 %. At 340°C, the quinoline moiety was lost in the third stage of breakdown, resulting in a 47.95 % weight loss. Furthermore, the compound disintegrated up to 492°C due to the loss of the remaining organic moiety. Cupric oxide is the final weight of the residue.

Antimicrobial activities

In vitro antibacterial activity of the prepared ligands and their copper complexes were tested on bacterial and fungal species. One day before the experiment, bacterial and fungal cultures were inoculated in broth (inoculation medium) and incubated at 37°C overnight. To ensure uniform distribution, the inoculation medium containing 24 h of produced crop was put to the nutrient medium and properly mixed. The solution was poured into petri plates and allowed to set at room temperature,

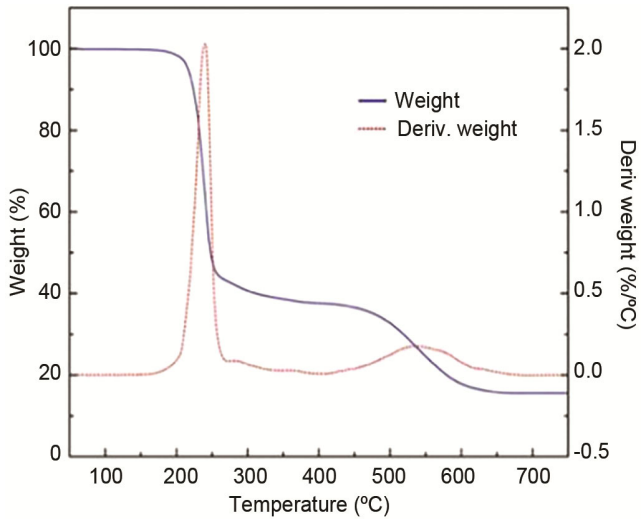

Fig. 4 — TGA and DTA curves of Cu (II) complex 3c

resulting in the production of gels. Wells (6 mm in diameter) were cut onto agar plates using sterile tubes. The wells were then filled to the agar surface with 0.1 mL of test chemicals dissolved in DMSO (200 μM / mL). The plates were let to stand for an hour to aid in the diffusion of the medication solution. The plates were subsequently incubated at 37°C for 24 h for bacteria and 48 hours for fungus, with the diameter of the inhibitory zones measured. Minimum inhibitory concentrations (MICs) were calculated using the serial dilution method. The MIC was determined to be the lowest concentration (μg / mL) of the drug that inhibits bacteria growth at 37°C after 24 h of incubation and fungal growth at 37°C after 48 h of incubation. The amount of DMSO in the medium had no effect on the growth of any of the bacteria examined.

Three Gram-negative bacteria, *Proteous vulgaris, Klebsiella pneumoniae, and Shigella flexneri,* three Gram-positive bacteria, *Staphylococcus aureus, Staphylococcus epidermidis, and Bacillis subtilis,* and three Fungi, *Aspergillus fumigatus, Aspergillus clavatus, and Canadia albicans,* were tested *in vitro* for antibacterial and antifungal activity. Table 2 and 3 summarized the minimum inhibitory concentration (MIC) values of ligands and their copper complexes. A comparative analysis of ligands and their complexes (MIC values) shows that the antimicrobial activity of copper complexes is higher than that of free ligands

Heteroaromatic residues may be responsible for the ligands' antibacterial action. Antimicrobial activity is higher in compounds with a C=N group than in compounds with a C=C group. The enhanced activity of the complexes can also be described using Overtone's notion [38] and Tweedy's chelation theory[39]. The lipid membrane that surrounds the cell, according to Overtone's idea of cell permeability, enables only lipid-soluble molecules to pass through, making liposolubility a key element in limiting antimicrobial action. Liposolubility is an important factor in reducing antibacterial activity. The polarity of the metal ion would be reduced to a greater degree during chelation due to the overlap of the ligand orbital and partial sharing of the positive charge of the metal ion with donor groups. It also increases the delocalization of π electrons around the entire chelate ring, which improves the lipophilicity of the complexes. Increased lipophilicity enhances complex penetration across lipid membranes and keeps metal binding sites in microorganism enzymes unblocked. These complexes

Table 2 — Minimum inhibitory of concentration of the synthesized compounds against growth of bacteria (Microgram per milliliter)

Ligand / Complex	Gram +ve bacteria			Gram -ve bacteria		
	B.subtilis	*S.epidermidis*	*S.aureus*	*S.flexneri*	*K.pneumonia*	*P.vulgaris*
2a	18.4	22.7	17.5	24.9	18.6	19.4
2b	25.4	24.6	18.7	23.4	19.8	20.2
2c	16.6	17.1	16.4	18.4	17.8	17.4
2d	17.9	21.7	17.9	21.4	19.1	18.2
2e	20.5	20.7	20.6	22.6	21.4	22.2
3f	20.9	22.3	23.4	22.7	22.7	22.5
2g	21.4	22.1	23.2	23.7	21.8	22.4
2h	22.7	22.5	21.8	21.6	22.2	22.3
2i	22.2	22.7	21.4	22.5	21.7	21.8
3a	5.9	6.4	6.1	6.9	7.9	7.5
3b	6.8	7.6	8.1	9.7	8.6	9.2
3c	4.6	5.7	5.5	7.4	7.6	5.5
3d	4.9	5.4	5.1	5.9	6.9	5.4
3e	7.4	7.3	8.2	7.8	8.3	7.6
3f	7.7	7.8	7.9	8.1	7.7	8.2
3g	8.3	8.4	8.8	9.2	8.6	8.4
3h	9.4	9.5	9.4	9.1	8.8	9.6
3i	8.4	8.5	8.8	8.7	8.7	9.1
Ampicilin	1.8	1.7	1.6			
Gentamycin				1.8	1.6	1.7

also interfere with the cell's respiratory system, impeding protein synthesis and so restricting the organism's ability to grow. Microorganisms die as a result. High solubility, particle fitness, metal ion size, and the presence of bulkier organic moieties all contribute to the complexes' higher antibacterial action. The development of a hydrogen connection between the active centre of cell components and the azomethine group disrupted normal cell function [40]. The observed variance in copper complex activity across the diverse types of species tested could be explained by differences in cell wall and/or membrane structure. Copper complexes are likely to have increased lipophilicity due to the lipophilic group C=N and the large heteroaromatic ring system of quinoline, allowing them to penetrate the cell wall and facilitate unfavourable intracellular interactions.

Because it features a chlorine substitution at the 7th position, complex 3c demonstrated the best activity against *Aspergillus fumigatus* of all the complexes evaluated in this study. In comparison to other complexes, this electron withdrawing group boosts lipophlicity and increases activity. Because this fungus is exceedingly hazardous to human. This shows that the molecular structure of the ligands and the type of complex generated affect antibacterial and antifungal action. The Cu (II) Schiff-base complex appears to have considerable antibacterial and antifungal activity, based on the preceding studies.

Table 3 — Minimum inhibition of concentration of the synthesized compounds against growth of fungi (Microgram per millimeter)

Ligand \ Complex	Fungi		
	C.albicans	*A.fumigatus*	*A.clavatus*
2a	19.4	19.7	20.4
2b	19.9	20.3	20.7
2c	18.4	18.9	18.6
2d	18.6	19.9	19.6
2e	20.4	20.7	20.4
2f	21.4	22.7	23.8
2g	21.9	22.7	21.9
2h	22.7	23.4	22.6
2i	22.4	23.2	22.7
3a	6.9	6.4	7.3
3b	7.7	7.1	7.8
3c	5.9	5.2	7.1
3d	6.7	6.4	6.9
3e	8.3	7.6	8.7
3f	8.9	8.4	10.7
3g	9.6	10.6	9.4
3h	10.4	9.4	10.2
3i	10.3	9.2	10.2
Amphotericin	2.3	2.8	2.4

Cell lines and cell culture

Cells were grown in RPMI 1640 media supplemented with 10% (v/v) heat-inactivated fetal bovine serum (FBS), 100 units/mL penicillin, and 100 g/mL streptomycin. Both cell lines were grown in culture at 37°C in a 5 percent CO_2 environment.

MTT cytotoxicity assay

The cytotoxicity against HL-60 and MCF-7 cell line was determined using the 3-[4,5-dimethyl-2-thiazolyl]-2,5-diphenyl-2H-tetrazolium bromide (MTT) test. This assay is based on MTT reduction by mitochondrial dehydrogenases in living cells. Cells were inserted in a 96-well sterile microplate (5 - 104 cells / well) and cultured for 48 h at 37°C in serum-free medium containing dimethyl sulfoxide (DMSO) and a series of various concentrations (12.5, 25, 50, and 100 mM) of each drug or doxorubicin prior to the MTT test (positive control). After incubation, the medium was withdrawn and 40 mL of MTT (2.5 mg/mL) was added to each well. The incubation time was extended for an additional four hours. The purple formazan dye crystals were dissolved in 200 mL of DMSO. The absorbance at 570 nm [41-43] was measured using a Spectra Max Paradigm Multi-Mode microplate reader. To calculate relative cell viability, the mean proportion of viable cells compared to control cells was employed. The synthesised complexes were evaluated in vitro for activity against HL-60 and MCF-7 cell line using the MTT assay Table 4. The percentage of undamaged cells was calculated and compared to the control. These compounds' activity against the two cell lines were compared to those of doxorubicin. All chemicals inhibited both cells in a dose-dependent manner. Ip[44] published comparative tests between comparable selenium and sulphur compounds, demonstrating that selenium inhibits cancer cell development far more effectively than sulphur. In addition, selenium may have a multi-modal mechanism for inhibiting cellular transformation. El-Bayoumi[45] eventually discovered evidence to support this hypothesis by expanding the studies to other comparable sulphur and selenium compounds. Synthesized complexes were investigated in this light. 3d, 3a, and 3b demonstrated moderate *in vitro* efficacy in terms of selectivity and as an orientative measure. At 100 mM, 3c was significantly more active than the control against two cell lines, HL-60 and MCF-7 shown in Fig. 5.

Table 4 — IC_{50} value of the nine products against the two cancer cell lines according to the MTT assay.

	% of inhibition	
Compound	HL-60	MCF-7
Doxorubicin	56.71	75.33
3a	54.43	70.52
3b	53.45	69.28
3c	56.72	72.82
3d	55.64	71.28
3e	53.34	66.42
3f	52.28	65.28
3g	51.85	63.32
3h	49.28	62.28
3i	49.35	61.3

Anti-inflammatory efficiency

Due to ethical concerns, purchasing and using animals for pharmaceutical research is a more difficult process. In light of these considerations, the current study focused on protein denaturation approach for *in vitro* anti-inflammatory efficiency of metal chelates using the egg albumin method. These chemical compounds may prevent protein denaturation, enhancing the anti-inflammatory action. When compared to Diclofenac (IC_{50} 50 g/mL), the produced copper chelate (IC_{50} 40 g/mL) displayed stronger inhibitory activity than other chelates (IC_{50} 78–90 g/mL) due to the presence of redox and chemical molecular moiety. The chelates' absorbance increased in comparison to the control, indicating that the protein was stabilising and thereby reducing the denaturation process. The biochemical interpretations revealed that the produced copper chelates were effective in reducing inflammation. Furthermore, clinical trials are required to determine the anti-inflammatory mechanism.

DNA binding studies

Absorption spectral studies

Electronic absorption spectroscopy was one of the most useful experimental techniques for studying metal ion-DNA interactions in metal complexes

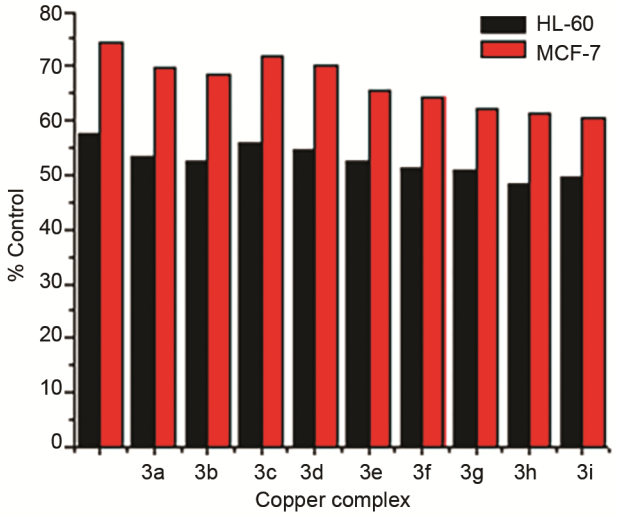

Fig. 5 — Cytotoxicity against two cancer cell lines. according to the MTT assay at 100 mM.

. Intercalation with DNA generally results in hypochromism and bathochromism due to the strong stacking interaction between aromatic chromophores and CT-DNA base pairs[46]. The absorption spectra demonstrate that the absorbance of complex 3c is clearly resolved at 289 nm. Increasing the concentration of CT-DNA resulted in hypochromic and bathochromic enhancements in its visible absorption spectra due to the formation of more stable complexes. In the presence of increasing CT-DNA concentrations, complex 3c demonstrated a decrease in intensity, as well as a shift towards higher wavelengths hypochromicity (approximately 11 %) and bathochromic alterations (maximum: 21.1 nm) for its highest red-shift absorption peak (Fig. 6) maxima. Using the change in absorbance values with increasing amounts of CT-DNA, the intrinsic binding constants (K_b) were calculated, and (K_b) was found to be 4.0×10^5 M^{-1}, showing that complex 3c binds firmly to CT-DNA through intercalation[47,48].

Fluorescence studies

In Tris buffer, the complex 3c produces luminescence with a maximum at 450 nm at room temperature (*p*H 7.0-7.2). The intensity of the emission increases when CT DNA (Calf thymus DNA) is added to the complex, relative to the intensity of the complex alone (Fig. 7). It has previously been observed that the addition of second molecules might attenuate this enhanced fluorescence, at least somewhat. This implies that the copper complex interact strongly with CT-DNA via intercalation and it will be effectively shielded by DNA, because the hydrophobic environment within the DNA helix restricts the accessibility of solvent water molecules to the duplex and thus restricts complex mobility at the binding site, resulting in a reduction in vibrational modes of relaxation[49], which increases the copper complex's degree of enhancement, which is consistent with the absorption spectra. The order of rise in complicated emission rate was supported by absorption spectra and viscosity measurements.

Viscosity measurements

The viscosity data helped to explain the copper complex's binding modes with CT-DNA. In the absence of crystallographic structural data, the most essential tests of binding in solution are hydrodynamic assays sensitive to length change (for example, viscosity, sedimentation) [50]. A conventional intercalative mode causes a significant rise in the viscosity of DNA solution due to an increase in base pair separation at intercalation sites and hence an increase in total DNA length. A compound that binds primarily in the DNA grooves by partial and non-classical intercalation, on the other hand, frequently generates a negative or no shift in DNA solution viscosity under the same conditions. By altering the concentration of the complex, viscosity measurements on CT-DNA were performed to better elucidate the binding mode of the current complex. The effects of the complex on the viscosity of rod-like DNA

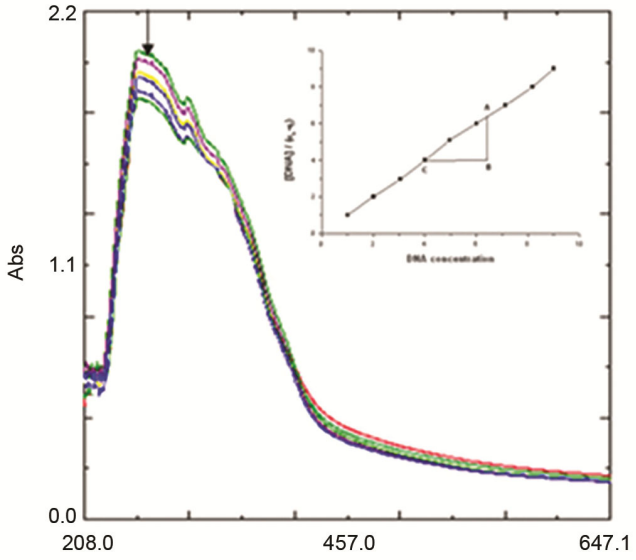

Fig. 6 — Absorption spectral traces of copper complex 3c in Tris HCl buffer (0.01M, pH 7.2) upon addition of CT-DNA=0.5 µm, =10 µm, drug, 20 µm; 30 µm; 40 µm; 50 µm; Arrow Shows the absorbance changing upon increase of DNA concentration.

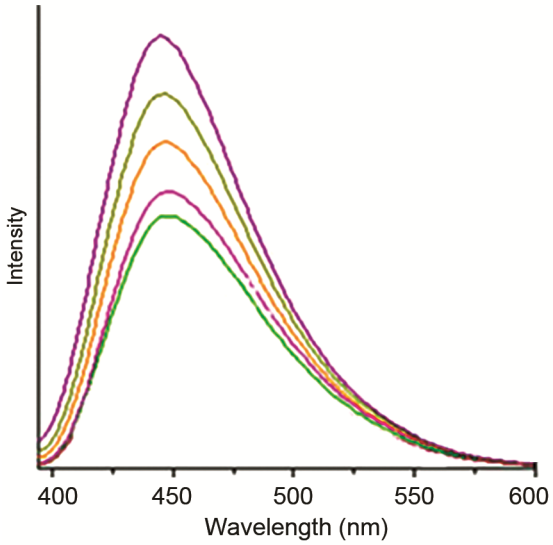

Fig. 7 — Fluorescence emission of copper complex 3c in Tri-HCl buffer. Fluorescence intensity increasing CT-DNA concentrations (5 µl, 10 µl, 15 µl, 20 µl……). Inset: plots of relative emission intensity versus [DNA]/[complex]

were illustrated in Fig. 8. The viscosity of DNA increases as the concentration of the complex 3c increases. As a result of the observations, the complex's presence has a demonstrable impact on CT-DNA relative viscosity.

α-Glucosidase inhibition

The study on α-glucosidase inhibition for copper (II) complexes was described in Table 5, reflecting the IC_{50} values. The chelation of various metal acetate with inactive produced a perceptible increase in the inhibitory potential of ligand α-glucosidase and demonstrated the vital function of copper (II) centre during enzyme inhibition. This research predicts the concentration- dependent inhibition of α-glucosidase induced by the copper complexes (II). Among the complexes tested, the copper (II) complex 3c was highly potent α-glucosidase inhibitors (IC_{50} = 0.20 μM) and was approximately 200 times more active than the DNJ (IC_{50} = 300 μM) standard α-glucosidase inhibitor. Copper (II) complex 3c was the most potent α -glucosidase inhibitor tested (IC_{50} = 0.18 μM) and was roughly 200 times more active than the DNJ (IC_{50} = 300 μM) standard -glucosidase inhibitor. The active site residues of α-glucosidases (imidazole and carboxy groups) interact with metal (II) ions through soft electron donors like imidazole nitrogen, which inhibits the enzyme. The presence and position of substituents in the compound $[Cu^3(OAc)_2]$ influence α-glucosidase inhibition. The inhibitory results indicate that the copper complex 3c can more easily occupy the active α-glucosidase sites than the conventional DNJ. As a result of its redox characteristics and molecular scaffolds, copper complex is an effective inhibitor of α - Glucosidase.

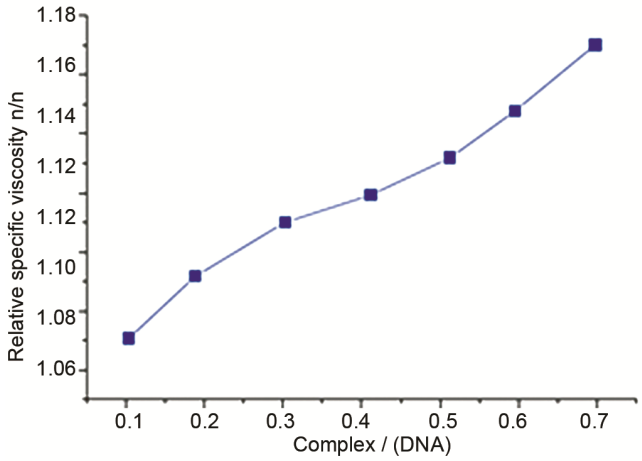

Fig. 8 — Effects of increasing amount of copper Complex 3c on the relative viscosity of CT-DNA at 25 ± 0.1ºC

Table 5 — α-Glucosidase inhibition activity of copper (II) complexes.

Complex/ Standard	IC_{50} (μM)
3a	0.50 ± 0.4
3b	0.82 ± 0.5
3c	0.20 ± 0.02
3d	0.54 ± 0.4
3e	0.95 ± 0.03
3f	0.82 ± 0.01
3g	1.09 ± 0.2
3h	1.10± 0.1
3i	1.11± 0.2
DNJ	300 ± 0.5

Cholinesterase inhibitory activity

Cholinesterase inhibitors (ChEIs) are a class of drugs that increase cholinergic activity in the brain to improve memory, efficiency, and reduce psychiatric and behavioural disorders. Using a modified Ellman method, the AChE and BuChE inhibitory activities of the synthesised phenylselanylquinoline derivative were determined and compared to Galantamine and Rivastigmine as standards. Some acetylcholinesterase inhibitors (donepezil, galantamine, and rivastigmine) were used to treat AD symptoms. Table 6 summarises the IC_{50} values for AChE and BuChE inhibitions. The heavily conjugated phenylselanylquinoline derivative, like ordinary Galantamine (IC_{50} = 2.40 μM), showed the highest inhibition against AChE with an IC_{50} value of 0.19 μM and Rivastigmine (IC_{50} = 3.01 μM). The IC_{50} values obtained showed that phenylselanyl quinoline derivatives, as opposed to Galantamine, serve as a selective inhibitor of AChE through a hydrophobic interaction and an interaction between π–π interactions. The fused aromatic nuclei with higher inhibitory AChE potencies are illuminated by the aromatic centre than their similar molecules with only one or two fused ring systems. The best inhibitors for acting as powerful AChE inhibitors have fused aromatic properties. The azomethine

Table 6 — *In vitro* inhibition IC_{50} values (μM) and selectivity index of compound and Standards for AChE and BuChE.

Compound	Inhibitory values IC_{50} (μM)		Selectivity index = IC_{50} (BuChE)/IC_{50} (AChE
	AChE	BuChE	
Ligand 2c	0.31 ± 0.12	3.0 ± 0.21	10
Galantamine	2.40 ± 0.10	17.30 ± 0.15	7.20
Rivastigmine	3.01 ± 0.20	0.30 ± 0.11	0.1

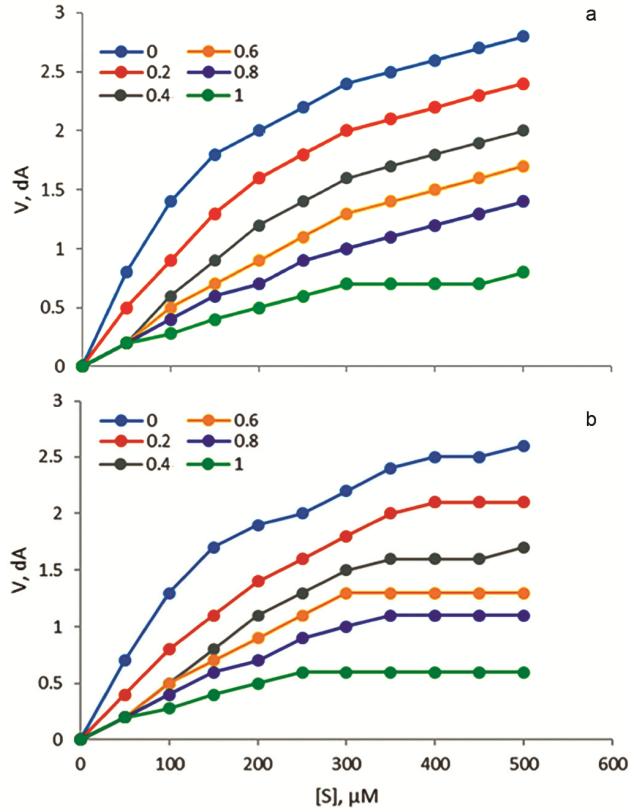

Fig. 9 — (b): Plot of BuChE initial velocity with increasing substrate concentration.

moiety also promotes tight binding to the AChE active site, effectively inhibiting choline substrate hydrolysis. As a result, the azomethine, quinoline, lipophilic moieties on conjugated aromatic centres, may be the primary prerequisite for anti-AChE activity. The inhibitory activities were attributed to the conjugated fused aromatic core moieties, according to the findings. Kinetic studies with AChE and BuChE, as well as ligand, were carried out to better understand the nature of their binding interactions. The ligand kinetic characteristics and inhibitory features were determined using the plot (Lineweaver–Burk reciprocal plot) representation. With AChE and BuChE, the observed K_m and V_{max} values of ligand 2c at different concentrations are mentioned. As can be seen in Fig. 9(a), increasing concentration changed both the slopes (lower V_m) and intercepts (higher K) (0.2, 0.4, 0.6 and 1.0 mM). This activity indicates that the ligand 2c inhibits AChE. As shown in Fig. 9(b), the ligand 2c inhibited BuChE and reduced the enzymatic velocity of catalytic BuChE-substrate reaction in a dose-dependent manner. The ligand could be bound to the catalytic active site and peripheral anionic site when engaging with therapeutic targets, according to these experimental results.

Conclusion

The synthesis, characterisation, and biological evaluation of copper (II) complexes with organoselenium based schiff base ligands ((16E)-N-(2-phenylquinolin-4(1H)-ylidine)-2-(phenylselanyl) pyridine-3-amine have been investigated in this study. Spectroscopic examinations reveal that the complex is connected with two carboxylate oxygen atoms and a copper atom via the quinoline moiety and organoselenium from the ligand. According to the analytical and spectral data, all copper complexes have a distorted square planar geometry with a metal to ligand ratio of 1:1. Absorbance, fluorescence and viscosity measurements have been used to evaluate the copper complexes' binding relationship with calf thymus DNA (CT-DNA). All of the complexes reacted with CT-DNA via an intercalation manner, according to these findings. According to the antimicrobial study, lipophilic and polar substituents like C=N and Se–N are likely to increase fungal and bacterial toxicity, and hence copper (II) complexes have a higher probability of interacting with nucleotide bases. Furthermore, it was discovered that complexing the ligand with the metal ion improves its anticancer activity in the MCF-7 cell line. When compared to the standard inhibitor (DNJ), the synthesised Cu (II) complex show effective inhibitory activity of α -glucosidase and could be used in the future for antidiabetic and other related disorders. They also contain Cholinesterase inhibitory action, which could be play a key role in the treatment of Alzheimer's disease in the future.

Acknowledgement

The authors thank the Head, Department of Chemistry, Manonmaniam Sundaranar University for providing the necessary facilities. This research did not receive any specific grant from funding agencies in the public, commercial, or not-for-profit sectors.

Disclosure statement

No potential conflict of interest was reported by the authors.

References

1 De Oliveira C Brum J, Neto D C F, de Almeida, J S F, Lima, J A, Kuca K, França T C C & Figueroa-Villar J D, *Int J Mol Sci*, 20 (2019) 3944.

2 Pinz M P, Dos Reis A S, Vogt A G, Krüger R, Alves D, Jesse C R & Luchese C, *Biomed Pharmacother*, 105 (2018) 1006.

3 Fiorito J, Saeed F, Zhang H, Staniszewski A, Feng Y, Francis Y I & Arancio O, *Euro J Med Chem*, *60* (2013) 285.
4 Abdel-Rahman L H, Abu-Dief A M, Aboelez M O & Abdel-Mawgoud, A A H, J *Photochem Photobiol*, *170* (2017) 271.
5 Abdel-Rahman L H, Abu-Dief A M & Abdel-Mawgoud Azza A H, *Int J Nano Chem*, 5 (2019)1.
6 Abdel-Rahman L H, Abu-Dief A M, Shehata M R, Atlam F M & Abdel-Mawgoud A A H, *App Organomet Chem*, 33 (2019) 4699.
7 Abdel-Rahman L H, Abu-Dief A M, Moustafa H & Abdel-Mawgoud A A H, *Arab J Chem*, 13 (2020) 649.
8 Abdel-Rahman L H, Abu-Dief A M, Adam M S S & Hamdan S K, *Catal Lett*, 146 (2016) 1373.
9 Al-Saeedi S I, Abdel-Rahman L H, Abu-Dief A M, Abdel-Fatah S M, Alotaibi T M, Alsalme A M & Nafady A, *Catalysts*, 8 (2018) 452.
10 Adam M S S, Abdel-Rahman L H, Abu-Dief A M & Hashem N A, *Inorg Nano-Met Chem*, 50 (2020) 136.
11 Huijbregts S C J, De Sonneville L M J, Van Spronsen F J, Berends I E, Licht R, Verkerk P H & Sergeant J A, *Neuropsychology*, 17 (2003) 369.
12 Lee E S, Choi B W, Jung D I, Hwang H J, Han J T & Lee B H, *B Korean Chem Soc*, 24 (2003) 243.
13 Fisher A, *J Neurochem*, 120 (2012) 22.
14 Chan K Y, Wang W, Wu J J, Liu L, Theodoratou E & Car J, *The Lancet*, 381 (2013) 2016.
15 Anand P, Singh B & Singh N, *Bioorg Med Chem*, 20 (2012) 1175.
16 Somani G, Kulkarni C, Shinde P, Shelke R, Laddha K & Sathaye S, *J Pharm Bioallied Sci*, 7 (2015) 32.
17 Tardito S & Marchio L, *Curr Med Chem*, 16 (2009) 1325.
18 Wessjohann L A, Schneider A, Abbas M & Brandt W, *Bio. Chem,* 388(10) (2007) 997.
19 May S W & Pollock S H, *Drugs*, 56 (1998) 959.
20 Mugesh G, du Mont W W & Sies H, *Chem Rev*, 101 (2001) 2125.
21 Marzano C, Pellei M, Tisato F & Santini C, *Anti Cancer Agents Med Chem*, 9 (2009) 185.
22 Santini C, Pellei M, Gandin V, Porchia M, Tisato F & Marzano C, *Che Rev*, 114 (2014) 815.
23 Zeglis B M, Pierre V C & Barton J K, *Chem Commun*, 44 (2007) 4567.
24 Gil A, Melle-Franco M, Branchadell, V & Calhorda M J, *J Chem Theory Comput*, 11 (2015) 2714.
25 Adhikary C, Bera R, Dutta B, Jana S, Bocelli G, Cantoni A & Koner S, *Polyhedron*, 27 (2008) 1556.
26 Patel R N, Kumar S & Pandeya K B, *J Inorg Biochem*, 89 (2002) 61.
27 Winterbourn C C, *Biochem J*, 198 (1981) 125.
28 Bansod A D, Mahale R G & Aswar A S, *Russian J Inorg Chem*, 52 (2007) 879.
29 Nakamoto. K, *Spectroscopy and Structure of Metal Chelate Compounds* (John Wiley, New York) (1988).
30 Geary W J, *Coordination Chem Rev*, 7 (1971) 81.
31 M Hamming M & Foster N, *Interpretation of Mass Spectra of Organic Compounds* (Academic Press, New York, wileyonlinelibrary.com/journal/aoc Copyright c_ 2011 John Wiley & Sons Ltd) (1972).
32 Liu Y J, Wang N, Mei W J, Chen F, He L X, Jian L Q & Wu F H, *Transit Met Chem*, 32 (2007) 332.
33 Chandra S & Gupta L K, *Spectrochim Acta A Mol Biomo Spectrosc*, 61 (2005) 269.
34 Lever A B P, *Inorganic Electronic Spectroscopy*, 2nd edn. (Elsevier, New York) (1968).
35 Gaballa A S, Asker M S, Barakat A S & Teleb S M, *Spectrochim Acta A Mol Biomo Spectrosc*, 67 (2007) 114.
36 Fujiwara M. Wakita H, Matsushita T & Shono T, *Bull Chem Soc Jpn*, 63 (1990) 3443.
37 Geary W J, *Coordination Chem Rev*, 7 (1971) 81.
38 Anjaneyulu Y & Rao R P, *Synth React Inorg Met Org Chem*, 16 (1986) 257.
39 Dharmaraj N, Viswanathamurthi P & Natarajan K, *Transit Me Chem*, 26 (2001) 105.
40 Anacona J R, Gutierrez C, Nusetti O & LoroÑo D, *J Coord Chem*, 55 (2002)1433.
41 Hamdy N A, Anwar M M, Abu-Zied K M & Awad H M, *Acta Pol Pharm Drug Res*, *70* (2013) 987.
42 Soliman H A, Yousif M N M, Said M M, Hassan N A, Ali M M, Awad H M & Abdel-Megeid F M, *Der Pharma Chem*, 6 (2014) 394.
43 Awad H M, Abd-Alla H I, Mahmoud K H & El-Toumy S A, *Med Che Res*, 23 (2014) 3298.
44 Ip C & Ganther H E, *Carcinogenesis*, 13 (1992) 1167.
45 El-Bayoumy K, Sinha R, Pinto J T & Rivlin R S, *J Nutri*, 136 (2006) 864S.
46 Bailey N A, de Barbarin C O R, Fenton D E, Hellier P C, Hempstead P D, Kanesato M & Leeson P B, *J Che Soc Dalton Trans*, 5 (1995) 765.
47 Prabhakara M C, Naik H B, Krishna V & Kumaraswamy H M, *Nucleosides Nucleotides Nucleic Acids*, 26 (2007) 459.
48 Lamani D S, Reddy K V, Naik H B, Naik H P & Naik L R, *Phosphorus Sulfur Silicon*, 185 (2010) 550.
49 Prakash Naik H R, Bhojya Naik H S, Ravikumar Naik T R, Naik H R, Lamani D S & Aravinda T, *J Sulphur Chem*, 29 (2008) 583.
50 Vaidyanathan V G & Nair B U, *J Inorg Biochem*, 95 (2003) 334.